S2-25

N91-24867

P.29

Production of Oxygen From Lunar Ilmenite

F. Shadman and Y. Zhao

Department of Chemical Engineering

The University of Arizona

Abstract

The kinetics and the mechanism of reduction of synthetic ilmenite by hydrogen in the temperature range of 807-1014°C were investigated. At temperatures below 876°C, the temporal profiles of conversion have a sigmoidal shape and indicate the presence of three different stages (induction, acceleration and deceleration) during the reduction reaction. The apparent activation energy for the reaction is 22.3 kcal/mole, whereas the intrinsic activation energy is 16.9 kcal/mole. Scanning electron microscopy and energy dispersive X-ray analyses show that the diffusion of Fe product away from the reaction front and through the TiO_2 phase, followed by the nucleation and growth of a separate Fe phase is an important step affecting the process kinetics. X-ray diffraction and wavelength dispersive X-ray results indicate that the TiO_2 can be reduced to lower oxides of titanium at temperatures higher than 876°C.

Introduction

Oxygen is a consumable material which needs to be produced continuously in most space missions. Its use for propulsion as well as life support makes oxygen one of the largest volume chemicals to be produced in space. Production of oxygen from lunar materials is of particular interest and is a very attractive possibility.

The solid state metallurgical processes for recovering metals from ores are important as potential replacements for conventional smelting and wet chemistry techniques. An industrially important process receiving a great deal of attention is the solid state separation of titanium dioxide and iron present in ilmenite (chemically iron titanate, $FeTiO_3$). In industrial practice, ilmenite or titanomagnetite ores are smelted with carbon in high temperature furnaces. This process produces pig iron and a titania-enriched slag. The pig iron can be employed for castings while the slag can be further processed to extract titanium dioxide. This conventional smelting route has a number of serious disadvantages. Firstly, the electric furnace smelting is energy intensive. Secondly, in the smelting processes, it is necessary to produce a fluid titania-enriched slag. Thus, in this case, slag-forming reagents, which lower the melting point and the viscosity of the slag phase, must be added. These additives dilute the concentration of titanium dioxide in the slag and have deleterious effects on the subsequent processes for extracting titania from the slag (Merk and Pickle, 1988). Therefore, it would be beneficial to develop a direct reduction

process which produces a solid slag and coarse iron particles which can be removed by either leaching or mechanical separation methods.

In recent years there has been a rising interest in the solid state reduction of ilmenite ores. This interest is linked with the process for winning oxygen from lunar materials (Cutler and Krag, 1985; Zhao and Shadman, 1989, 1990). Ilmenite, a mineral found in substantial quantities in lunar maria (Lewis, 1987) is an attractive source of oxygen because of its relatively low reduction temperature as compared to silicon, aluminum, titanium, calcium or magnesium oxides in the lunar soil. Iron oxide reduction can also produce iron and titanium dioxide as co-products. In addition, Agosto (1986) has concluded that ilmenite can be obtained from lunar soil at high purity using electrostatic separation techniques. The ilmenite may be heated with hydrogen gas (brought up from the earth) in the temperature range of 600°C to 1000°C. The products are water vapor and an intimate, and probably sintered, mixture of solid metallic iron with titanium dioxide (the mineral rutile). The water vapor is condensed and dissociated by electrolysis. The products of electrolysis are oxygen which is liquefied for use as a propellant and for life support, as well as hydrogen, which is recycled through the ilmenite reactor.

Most previous studies have been on naturally occurring ores using carbon or CO as reducing agents (Wouterlood, 1979; Jones, 1975). From a fundamental point of view, the results of such studies are difficult to interpret because of the complex nature of the ores, the presence of many components, and the inherent variations in ore composition. Consequently, the fundamental kinetics and mechanism of ilmenite reduction by hydrogen are not well understood. Briggs and Sacco (1988) studied the reduction of ilmenite by hydrogen at 600°C and 800°C. The ilmenite used in their study contained about 8% ferric iron. They found that some preoxidation of ilmenite by oxygen prior to reduction can decrease the complete reduction time of samples. During preoxidation, the ilmenite is converted to pseudobrookite (Fe_2TiO_5) and rutile. The single crystals of ilmenite are converted, therefore, into a polycrystalline array of pseudobrookite and a fine dispersion of rutile (Barnes and Pickles, 1988). Carbotek (1988) has developed a fluidized-bed reactor for the reduction of ilmenite by hydrogen at the temperature between 900°C and 1000°C. Terrestrial ilmenite was used in this study. They demonstrated the feasibility of producing oxygen from terrestrial ilmenite by first reducing the terrestrial ilmenite and then electrolyzing water to produce oxygen and hydrogen which is returned to the reactor. They also reported that the reaction is first order with respect to hydrogen under their experimental conditions. Bardi *et al.* (1987) investigated the kinetics of hydrogen reduction of Norwegian ilmenite ore powders. They found that the activation energy value of a surface chemical reaction was 34.8 kcal/mole in the temperature range of 654°C-1007°C. The electron microprobe analysis of the reduced Norwegian ilmenite grains showed the existence of a segregated iron phase present as spheroidal nodules and a TiO_2 phase present as vein-like arrangements. Their optical

microscopic study on sections of synthetically prepared $FeTiO_3$ showed separate reacted and unreacted zones in the sample particles.

The purpose of the present study is to obtain fundamental information on the kinetics and the mechanism of ilmenite reduction by hydrogen under conditions where the original ilmenite and the final products are well characterized. The emphasis is on ilmenite with no ferric impurities present. This is important in applying the results to the reduction of lunar ilmenite.

In this phase of the work the emphasis has been on the kinetics and mechanism of simulated lunar ilmenite reduction by hydrogen and H_2/CO, the comparison of H_2 reduction with CO reduction and the development of a novel process flowsheet for the carbothermal reduction of lunar ilmenite.

Experimental Approach

A schematic diagram of the experimental apparatus is shown in Figure 1. The main components of this system are an electronic microbalance (Cahn Instruments, Inc., Model 1000), a quartz flow through reactor, and a movable furnace with a PID temperature controller. The composition of the gaseous reactants was determined using gas chromatography. Ilmenite was used in the form of thin flakes pressed from powder. Samples were suspended from the microbalance, which allowed monitoring weight changes during the course of an experiment. A thermocouple was used to monitor the temperature of the reactor around the flake. All experiments were performed under isothermal conditions at temperatures between 807°C and 1014°C. The reducing gas entering the reactor was a mixture of H_2 and N_2. The gas flow rate was 660 std.cc/min, except in the experiments conducted to determine the effect of interphase mass transfer on the reduction rate.

Samples of starting material were prepared by cold pressing 0.270 g of $FeTiO_3$ powder (with particles size less than 45 μm) in a 12.2 mm diameter die at 552 MPa for 5 minutes to form disks. The disks were then cut into flakes approximately 10 mm by 8 mm. The thickness of the disks was 0.60 mm.

Each experiment was started by first purging the reactor system at room temperature to reduce the concentration of oxygen to levels below 10 ppm. A mixture of H_2/N_2 was then introduced into the reactor. To initiate the reduction, the furnace was raised rapidly. In less than three minutes, the temperature of the reaction zone was within 1% of the set point temperature. The experiments were terminated at a desired conversion by lowering the furnace.

Several techniques were used for chemical analysis and characterization of the starting material and the reduced samples. Mossbauer spectroscopy was employed to determine the oxidation state of iron in our synthetic ilmenite. X-ray diffraction (XRD) with a cobalt Ka source was used to identify the different crystalline phases in the starting material and the products. High-

resolution scanning electron microscopy (SEM), energy-dispersive X-ray (EDX) and wavelength-dispersive X-ray (WDX) analyses were employed to examine the polished cross section of both partially and completely reduced samples and to determine the elements present in each phase. For SEM, EDX and WDX analyses, the samples were mounted in an epoxy resin and polished to expose the cross-section of the grains.

Theoretical Approach

A mathematical model is formulated to describe the simultaneous reaction and diffusion that occur in the ilmenite flakes used in the experimental part of this study. The flakes were uniform and thin; therefore, the geometry assumed for mathematical modelling is that of an infinitely long and wide slab. This configuration was selected because it gives the desired information on the kinetics of ilmenite reduction without complications of sample shape. Thin flakes are also suitable for polishing as needed in the microprobe studies. It is assumed that the flakes consist of spherical and equal-sized grain particles of ilmenite. Based on the SEM micrographs and image analysis of grains in a flake, the overall size of a flake and the size of an individual grain do not change significantly during the reaction.

The reaction considered is as follows:

$$FeTiO_3(s) + H_2(g) = H_2O(g) + Fe(s) + TiO_2(s)$$

The following additional assumptions are made:

(1) The pseudo-steady state approximation is appropriate for describing the concentration of the gaseous species within a flake.
(2) The system is isothermal.
(3) The effective diffusivities of gaseous reactant and product are equal and uniform throughout the flake.
(4) The reaction is first order with respect to H_2 and H_2O.
(5) The grain particles have little porosity and react following a shrinking-core mechanism.

The conservation equations for hydrogen, A, and water, C, can be written as follows:

$$D_e\nabla^2 C_A - R_A = 0 \qquad (1)$$

$$D_e\nabla^2 C_C + R_A = 0 \qquad (2)$$

The local rate of reaction based on the grain particles is given by the standard shrinking core model:

$$-\rho_s \frac{dr_c}{dt} = k \frac{C_A - C_c/K}{1 + \frac{k(1+1/K)}{D_{eg}} (1 - \frac{r_c}{r_s}) r_c} \quad (3)$$

Dividing Equation (2) by K and subtracting from Equation (1) gives:

$$D_e \nabla^2 (C_A - C_c/K) - R_A (1 + 1/K) = 0 \quad (4)$$

The initial and the boundary conditions for (3) and (4) are

at t=0 $r_c = r_s$ (5)

at Z=L $C_A - C_c/K = C_{Ab} - C_{cb}/K$ (6)

at Z=0 $\frac{d(C_A - C_c/K)}{dZ} = 0$ (7)

An expression can be obtained for the local rate of reaction RA. For a flake in this study, RA is given by:

$$R_A = 3 \frac{r_c^2}{r_s^3} \frac{(1-\varepsilon)\, k\, (C_A - C_c/K)}{1 + \frac{k(1+1/K)}{D_{eg}} r_c (1 - \frac{r_c}{r_s})} \quad (8)$$

The local conversion can be related to the unreacted grain radius as follows:

$$X_B = 1 - (\frac{r_c}{r_s})^3 \quad (9)$$

The overall conversion for a flake is given by:

$$X = (\frac{1}{L}) \int_0^L X_B \, dZ$$

The solution to the model equations was obtained using the method given by Szekely *et al.* (1976). The method involves some approximation but is proven to represent the exact solution that must be obtained numerically.

Results and Discussion

The impurity content of the ilmenite used in this study is given in Table 1. The XRD pattern of this ilmenite, as shown in Figure 2, suggests that the only crystalline phase in the sample is $FeTiO_3$. Mossbauer spectra of the sample shows that the ilmenite used in this study contains only Fe^{++}. This represents the oxidation state of iron in lunar ilmenite.

Table 1. Maximum Impurity Content in the As-Received Synthetic Ilmenite*

Impurity	Maximum Concentration (Wt%)
Al	0.001
Ca	0.01
Cr	0.001
Cu	0.01
Mg	0.001
Si	0.1

* CERAC, Inc.

For each experiment, the temporal profile of conversion was determined by monitoring the sample weight using a recording electrobalance. Initially, some experiments were conducted to determine the effect of transport resistance in the interphase around the flakes. The experiments were conducted at the highest temperature (1014°C) with 3.4% H_2. The results showed that the interphase resistance is not important if the flow rate is at least 660 std.cc/min. At temperatures below 1014°C, the interphase resistance is even less significant.

The results in Figure 3 show the effect of H_2 concentration on the reaction at 945°C. The H_2 concentration was varied between 3.4% to 14.7% in N_2 atmosphere. As expected, an increase in the hydrogen concentration results in an increase in the rate and a decrease in the time required to attain certain fractional weight loss, which is defined as the ratio of weight loss of the sample to initial weight of the sample. The reaction order with respect to H_2 is established using the runs which were not influenced by diffusion in the ilmenite flake. The results, shown in Figure 4, indicate that the reaction order is unity in the H_2 concentration range of 3.4% to 14.7% at 807°C and 876°C. This confirms the first order kinetics assumption presented in the theoretical section.

Isothermal weight loss measurements were performed at 807, 876, 945 and 1014°C. The temporal profiles of conversion at these four temperatures and H_2 concentration of 3.4% are shown in Figure 5. The profile at 807°C has a sigmoidal shape and indicates the presence of three different stages (induction, acceleration and deceleration) during the reduction reaction. The profiles at 876°C, 945°C and 1014°C do not have these three stages. As shown in Figure 5, the time required to attain the weight loss corresponding to 'complete iron metallization' when all

the iron in ilmenite is reduced to metallic iron, is 210 minutes at 807°C and 52 minutes 1014°C with 3.4% H_2. The effect of temperature on the reaction rate is shown in Figure 6. The apparent activation energy calculated based on initial rates is 22.3 kcal/mole.

The model formulated in the previous section was used to extract intrinsic reaction rate constant from the experimental measurements. A list of parameters used in the model is given in Table 2. The model agrees well with the experimental measurements. Sample results for model predictions at 945°C and 1014°C are shown in Figures 7 and 8. The Arrhenius plot based on the intrinsic reaction rate constants is shown in Figure 9. The intrinsic activation energy for the reaction on ilmenite core is 16.9 kcal/mole. The fact that apparent activation energy is higher than the intrinsic activation energy is unusual and intriguing. This observation is related to the initial induction period and will be explained later.

Table 2. Values of Model Parameters

Parameter (unit)	Value
ε	0.33
ε_m	0.19
r_s (gmol/cm^3)	0.032
Average r_s (cm)	$7.2 \cdot 10^{-4}$
Thickness of flake (cm)	0.06
D_e (cm^2/sec)	1.040 (1014°)
	0.950 (945°C)
D_{eg} (cm^2/sec)	0.034 (1014°C)
	0.033 (945°C)
K	0.11 (1014°C)
	0.09 (945°C)

To gain insight into the mechanism of the ilmenite reduction, samples of both completely and partially reduced ilmenite were analyzed using various analytical techniques. In particular, a combination of optical microscopy, SEM, EDX, WDX and XRD analyses provided very useful information on the nature and the distribution of various solid products.

SEM backscattered electron micrographs of the polished cross-section of ilmenite flake after partial reduction at 1014°C and 807°C are shown in Figures 10a and 11a. The micrographs reveal three distinct regions which appear as bright, light gray and dark gray phases. In order to identify

these phases, quantitative EDX was performed at spots marked in Figures 10a and 11a. These results and the XRD observations (to be discussed later) show that the bright phase is primarily iron; the dark gray phase is titanium dioxide and the light gray phase is unreacted $FeTiO_3$. These results suggest that there is a strong tendency towards the segregation of the products iron and titanium dioxide, and that iron diffuses out of the grain particles through the TiO_2 layer during the reduction. This finding has important implications for product separation and recovery of Fe and TiO_2 from ilmenite, particularly for the application of magnetic seperation method.

Since the reduction temperatures are much lower than the melting point of TiO_2, The TiO_2 product is expected to be in polycrystalline form. Figure 10a and 11a indicate that the reaction in the grain particles proceeds according to the shrinking core model. This is because the grain particles of synthetic ilmenite are nearly nonporous, whereas the product TiO_2 is porous. The corresponding X-ray map of iron and titanium, shown in Figures 10b, 10c, 11b and 11c, confirm the shrinking core configuration. Moreover, SEM micrograph in Figure 11a indicates that hydrogen penetrates more into the unreacted ilmenite at 807°C than at 1014°C. The polished cross-sections of synthetic ilmenite flakes after complete reduction at 876°C and 945 °C were also examined by SEM and EDX. The results obtained at 945°C, as shown in Figures 12, confirm the complete segregation of products iron and titania. The EDX analyses of these samples indicate that the phase enriched in titanium is depleted in iron and vice versa.

In an earlier study in our laboratory, the kinetics and mechanism of ilmenite reduction with carbon monoxide were investigated (Zhao and Shadman 1990). The results showed that the reduction of TiO_2 did not take place at any appreciable rate in the temperature range of 800°C to 1100°C. However, the experimental results for the ilmenite reduction by hydrogen in Figure 3 show that the total weight loss of the sample exceeds the weight loss corresponding to 'complete iron metallization'. This indicates that titanium dioxide can be reduced by hydrogen in the temperature range of 876°C to 1014°C. The rate of reduction of titanium dioxide depends on both the hydrogen concentration and the reaction time. The reduction of titanium dioxide has practical significance in the production of oxygen from lunar ilmenite, since 67% of oxygen in ilmenite is bound to titanium.

In order to understand the mechanism of titania reduction by hydrogen, the electron microprobe with wavelength dispersive X-ray analysis was employed to determine the atomic ratio of oxygen to titanium in the reduced titanium dioxide phase. The analyzed area of the grain in the sample reduced at 1014°C is shown in Figure 13. For each sample, the analyses for titanium and oxygen were performed across the two polished grains. One is located at the edge of the flake; the other is located at the center. The results obtained from these two grains are very similar. The results showing the extent of reduction of TiO_2 are given by Figure 14 and indicate that the

reduction of titania took place throughout the titanium dioxide matrix in each grain. These observations suggest that the reduction of titanium dioxide in each grain and across the flake is kinetically controlled.

Another important point related to the reduction of TiO_2 is its inception relative to iron reduction. To further study this, two partially reduced samples were prepared at 1014°C and 14.7% H_2, the first one at 35% conversion and the second one at 70% conversion. The results of WDX analysis showed that the TiO_2 phases in both samples had not been reduced at either conversions. These results indicate that the reduction of TiO_2 does not occur to any significant extent as long as iron metallization is not completed. It is speculated that this is related to inhibition effect of water vapor as the reaction product. During ilmenite reduction (iron metallization), the concentration of water vapor inside the TiO_2 pores is high enough to inhibit the TiO_2 reduction. However, as iron metallization approaches completion, the inhibition effect decreases and TiO_2 reduction starts. The mechanism of H_2O inhibition is not known and is currently under study.

The XRD spectra of partially reduced samples are shown in Figure 15b. The phases present after partial reduction at 807°C and 1014°C are iron, titanium dioxide and unreacted ilmenite. Figure 15a is the XRD spectrum of sample reduced at 807°C with 'complete iron metallization', and indicates the presence of Fe and TiO_2. The samples reduced at 876°C, 945°C and 1014°C with 13% fractional weight loss were also analyzed using XRD. The patterns, shown in Figure 15c, indicate that all the peaks of TiO_2 phases disappeared, which confirms the reduction of TiO_2 by H_2.

The various observations described here point to a mechanism consisting of the following main steps for the reaction in each grain:

1. Diffusion of H_2 through the porous product layer of titanium oxide towards the unreacted core of the grain particles.
2. Reaction of H_2 with the ilmenite core to produce TiO_2 and Fe.
3. Migration of Fe through the TiO_2 layer away from the unreacted core towards the grain boundary.
4. Formation of iron nuclei and their subsequent growth outside and around the reacted grain particles.
5. Further reduction of TiO_2 to lower oxides of titanium by hydrogen.

Steps 3 and 4 result in almost complete segregation of the two solid products, iron and titanium dioxide, on the scale of grains.

An important point concerns the driving force behind the migration of iron followed by its nucleation and growth around the grain particles. Iron produced during the reduction reaction is distributed in the pores of the product rutile and has a higher activity than the agglomerated pure

iron mass outside the grain particles. This is related to the fact that the small iron islands on the surface are less stable and move towards a large iron mass to agglomerate. Thermodynamically, this minimizes the total surface energy.

Using the proposed mechanism, the sigmoidal profiles of conversion and the three stages observed during ilmenite reduction can be described as follows:

i) Induction stage : This represents the initial stage of the reduction process when the reaction rate is relatively low. The induction period is significant and observable at low temperatures. The induction period is definitely a genuine feature of the reaction mechanism and is not due to a delay in heating or similar experimental errors. A possible mechanism for the observed induction stage is the delay in the nucleation and growth of the iron phase. Initially, the iron produced by the reaction accumulates in the porous structure of the TiO_2 product layer. In this stage, the rate of iron production is faster than the rate of iron transport out of the TiO_2 layer. Consequently, TiO_2 pores are partially plugged and H_2 access to the reaction front is restricted. The induction stage is also present in the reduction of ilmenite by CO (Zhao and Shadman, 1990). However, the induction stage in the H_2 reduction ilmenite is less significant than that in CO reduction. This is because hydrogen diffusivity in the pores is significantly larger than CO diffusivity. Therefore, the effect of pore blockage on H_2 reduction is less than that on the CO reduction.

ii) Acceleration stage : As the reaction goes on, more iron is produced and transported to the grain boundaries , forming new nuclei and increasing the growth rate of iron phase. This facilitates the transport of the iron and opens up the TiO_2 pores. Consequently, H_2 transport to the reaction front is enhanced and an increase in the reaction rate is observed. It is important to note that the rise in rate during the second stage is not due to any autocatalytic effect of iron accumulation. The nucleation and accumulation of iron is outside the grain particles and not on the reaction surface. The accumulated iron and the reaction interphase are separated by a layer of non-reactive titanium dioxide.

iii) Deceleration stage: Finally, depletion of $FeTiO_3$ results in a decrease in the rate of reduction.

The results indicate that the intrinsic rate is influenced by the pore blockage effect particularly at low temperature. As temperature increases, the iron mobility, nucleation and growth are enhanced and the pore blockage effect becomes less significant. This causes an increase in the observed initial rate which is separate and in addition to the usual increase in rate caused by increasing temperature. Due to these dual effects of temperature, the apparent activation energy calculated from the initial rate data is higher than the intrinsic activation energy.

Shomate *et al.* has shown that the theoretically possible conversions for the reduction of ilmenite by CO are 5.1, 6.6 and 7.8 percent at 827°C, 1027°C and 1227°C, respectively. At the

same temperatures, the theoretically possible conversions for the reduction of ilmenite by H_2 are 5.1, 10.5 and 16.7 percent. Both carbon monoxide and hydrogen would be present in the gaseous stream if the process for the production of oxygen from ilmenite is based on the use of carbonaceous waste as a carbon source. Therefore, it is very important to compare the reduction of ilmenite by CO with the reduction of ilmenite by H_2.

The mechanisms of ilmenite reduction by H_2 and CO are very similar. Both reactions involve the migration and nucleation of iron, leading to the complete segregation of iron from TiO_2. The main difference between these two reactions is that TiO_2 can be reduced to lower oxides of titaniun by hydrogen and the reduction rate of ilmenite by H_2 is faster than that of ilmenite by CO.

The effect of temperature on both reactions is shown in Figure 16. The apparent activation energy for H_2 reduction of ilmenite is 22.3 kcal/mol, whereas the apparent activation energy for CO reduction of ilmenite is 29.6 kcal/mol. This suggests that the reduction of ilmenite by CO is more sensitive to temperature than that by H_2.

In order to determine the effect of reducing agents on the reaction rate and the time corresponding to the 'complete iron metallization', two sets of experiments were conducted at the same condition. The results in Figures 17 and 18 show that the initial reaction rates of ilmenite reduction by H_2 are 8.6 and 11.3 times larger than those by CO reduction at 1000°C and 900°C , respectively. The times corresponding to the 'complete iron metallization' are 12.5 minutes and 34 minutes at 1000°C and 900°C for H_2 reduction of ilmenite, whereas, for the CO reduction of ilmenite, times are 95 minutes and 135 minutes at 1000°C and 900°C.

The flowsheet for a novel carbothermal reduction process has been developed and is shown in Figure 19. The components and their funtions in this flowsheet are described as follows:

(1) Carbon monoxide generation section.

(2) Reactor with lower operation temperature: This reactor is designed to deposit carbon on lunar ilmenite. The thermodynamic calculation indicates that the deposit of carbon on lunar ilmenite can increase the oxygen yield significantly.

(3) Reactor with higher operation temperature: This reactor is to carry out the carbothermal reduction of lunar ilmenite. The major products in this reactor are Fe, TiO_2, CO and CO_2.

(4) Oxygen production section.

The staged reactor system with carbon deposition and reduction occurring at two different temperatures is a novel scheme that overcomes the inherent yield deficiency in other ilmenite reduction process.

In view of the presence of both CO and H_2 in ilmenite reduction process based on the use of carbonaceous waste and due to the technical advantages in ilmenite reduction by H_2/CO, the kinetics and the mechanism of ilmenite reduction by H_2/CO is currently under study. The preliminary result is shown in Figure 20.

Acknowledgment

This research was supported by NASA/UA Center for Utilization of Local Planetary Resources at the University of Arizona. The NASA/UA Graduate College Fellowship for Y. Zhao is gratefully acknowledged. Discussions with Dr. A. H. Cutler are very helpful in this study.

Registry No. $FeTiO_3$(Ilmenite), 12168-52-4; Fe(Iron), 7439-89-6; TiO_2(Rutile), 1317-80-2.

Nomenclature

C_A: concentration of H_2, gmol/cc

C_{Ab}: concentration of H_2 in bulk gas, gmol/cc

C_C: concentration of H_2O, gmol/cc

C_{Cb}: concentration of H_2O in bulk gas, gmol/cc

D_e: effective diffusivity in macro-pores in flake, cm^2/sec

D_{eg}: effective diffusivity in the micro-pores of product layer in each grain, cm^2/sec

E: intrinsic activation energy, kcal/mole

E_{app}: apparent activation energy, kcal/mole

k: surface reaction rate coefficient, cm/sec

k_{app}: apparent reaction rate coefficient, mg reacted · L/original mg · min mol

K: equilibrium constant

L: half thickness of the slab, cm

R_A: reaction rate, gmol H_2/cm^3 bulk flake · sec

Rate: reaction rate, mg reacted/original mg · min

r_c: radius of unreacted core in each grain, cm

r_s: radius of grain, cm

t: time, sec

T = temperature, °K

X_B: conversion of each grain

X: overall conversion of flake

Z: distance from the center of the slab, cm

Greek Symbols

ε: macro porosity

ε_μ: micro porosity

ρ_s: ilmenite molar density, $gmol/cm^3$

Literature Cited

- Agosto, W.N.; *Electrostatic Concentration of Lunar Soil Minerals*; In *Lunar Bases and Space Activities of The 21st Century*; edited by W. Mendell, Lunar and Planetary Institute, **1980**, 453.

- Bardi, G.; Gozzi, D.; Stranges, S.; *High Temperature Reduction Kinetics of Ilmenite by Hydrogen*; *Mater. Chem. and Phys.*, **1987**, 17, 32.

- Barnes, C.; Pickles, C.A.; *A Thermogravimetric Studies of The Catalytic Effect of Alkali Carbonates on The Reduction of Ilmenite*; *High Temp. Technol.*, **1988**, vol. 6 No 4, 195.

- Briggs, R. A.; Sacco, J. A.; *Oxidation and Reduction of Ilmenite: Application to Oxygen Production on the Moon*; Symposium sponsored by NASA, Houston (**1988**), paper No. LBS-88-170.

- Cutler, A.H.; Krag, P.; *A Carbothermal Scheme for Lunar Oxygen Production*; in *Lunar Bases and Space Activities in the 21st Century*, edited by W. Mendell, **1985**, 559.

- Lewis, J.S.; Lewis, R.A.; *Space Resources, Breaking the bonds of Earth;* Columbia University Press, New York, **1987**, 200.

- Merk, R.; Pickles, C.A.; *Reduction of Ilmenite by Carbon Monoxide; Can. Metall. Q.*, **1988**, vol. 27 No. 3, 179.

- Gibson, M.A.; Knudsen C.A.; Roeger, A.; *Development of The Carbotek Process for Lunar Oxygen Production; Engineering, Construction, and Operations in Space Conference,* Albuquerque; New Mexico, April 23-26, **1990**.

- Shadman, F.; Zhao, Y.; *Production of Oxygen from Lunar Ilmenite;* Annual Process Report, NASA/UA Center for Utilization of Local Planetary Resources, (**1988-1989, 1989-1990**).

- Szekely, J.; Evans, J.W.; Sohn, H.Y.; *Gas-Solid Reaction*, Academic Press, **1976**.

- Wouterlood, H.J.; *The Reduction of Ilmenite with Carbon; J. Chem. Tech. Biotechnol.*, **1979**, 29, 603.

• Zhao, Y.; Shadman, F.; *Kinetics and Mechanism of Ilmenite Reduction with Carbon Monoxide; AIChE* Journal, **1990**, vol. 36, No. 9, 443.

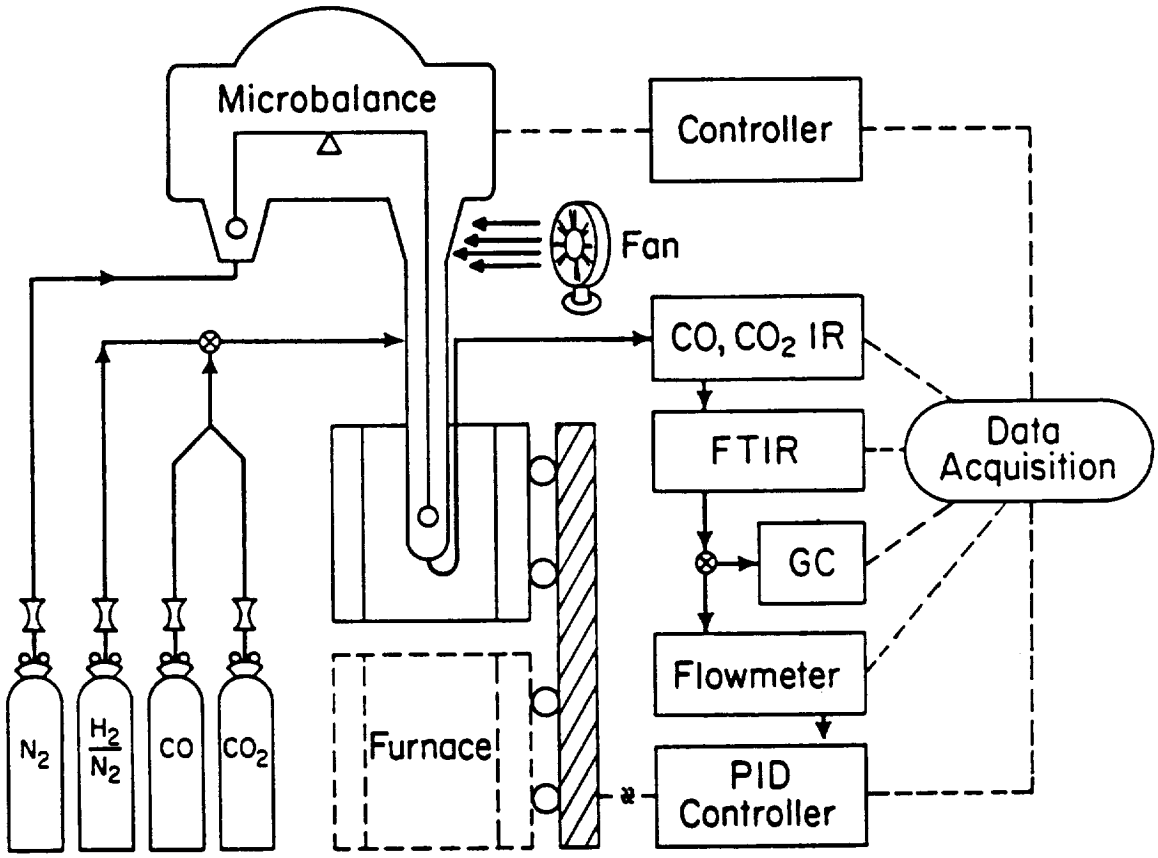

Figure 1. Schematic diagram of the reactor system. GC=gas chromatograph, IR=non-dispersive infrared analyzer, FTIR=Fourier transform infrared spectrometer

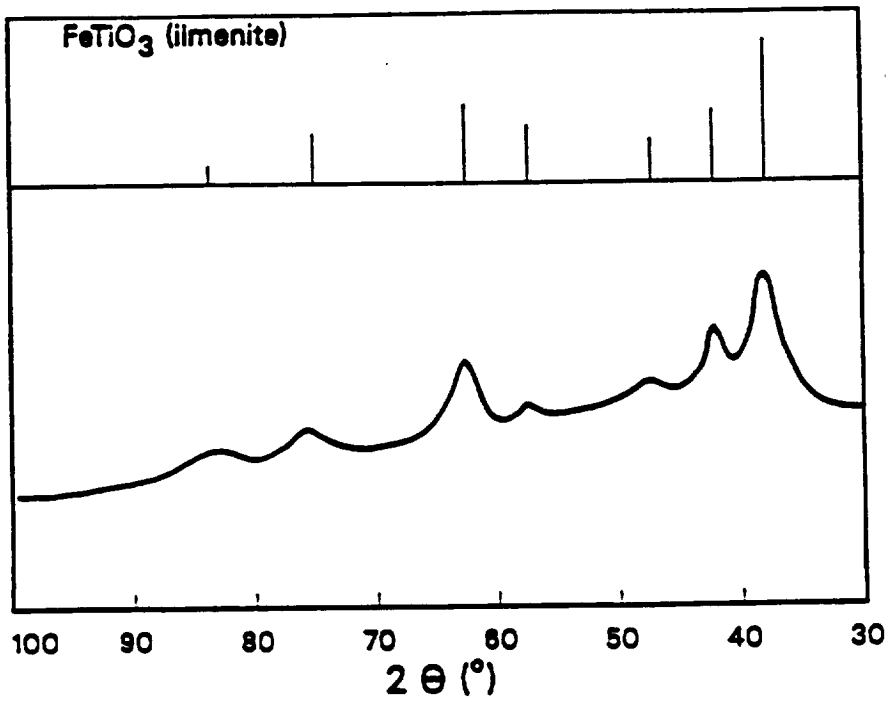

Figure 2. X-ray diffraction spectrum of synthetic ilmenite.

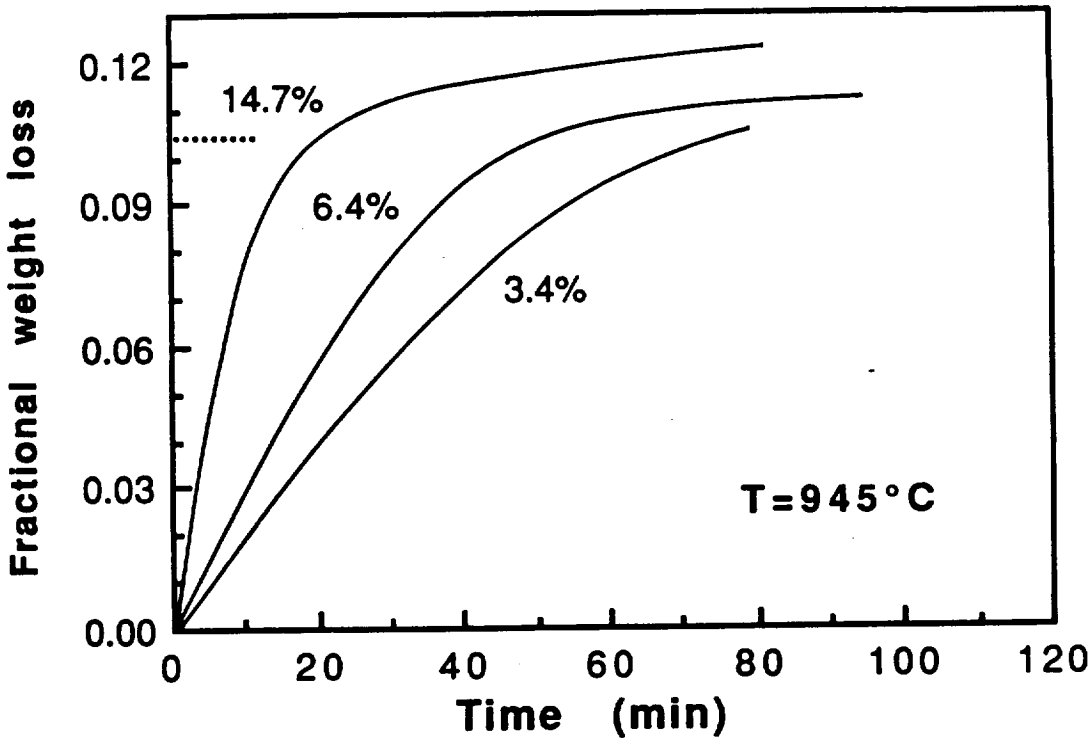

Figure 3. Effect of hydrogen concentration on the reduction of ilmenite; ·····, complete iron metallization.

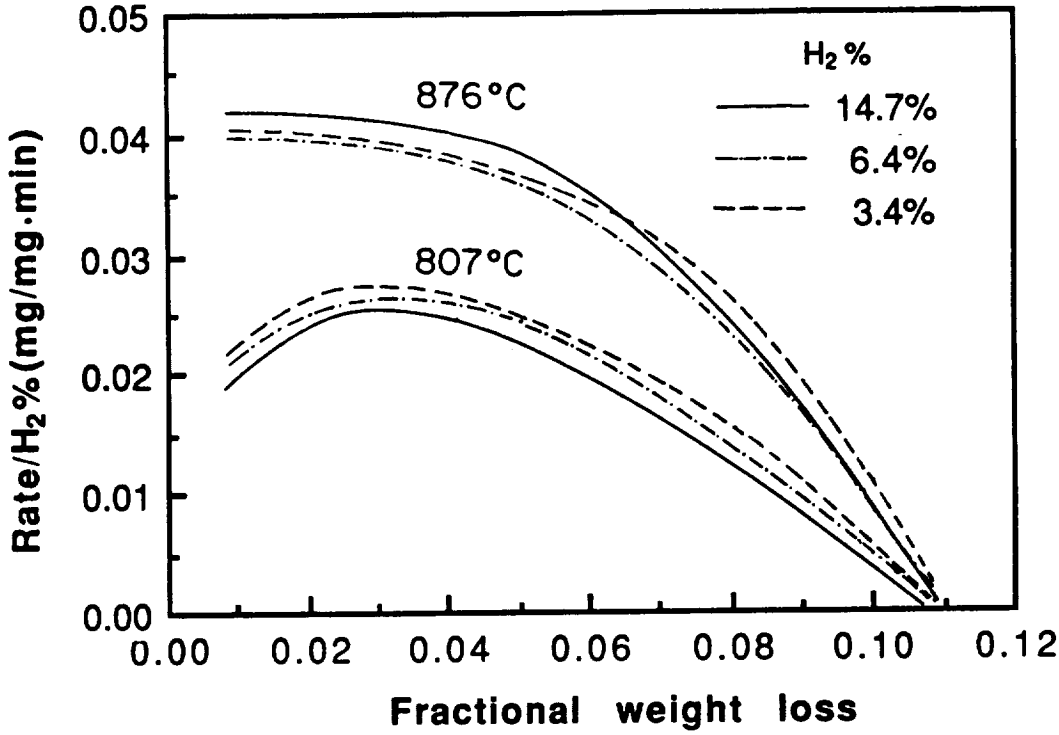

Figure 4. Effect of hydrogen concentration on the reduction rate of ilmenite

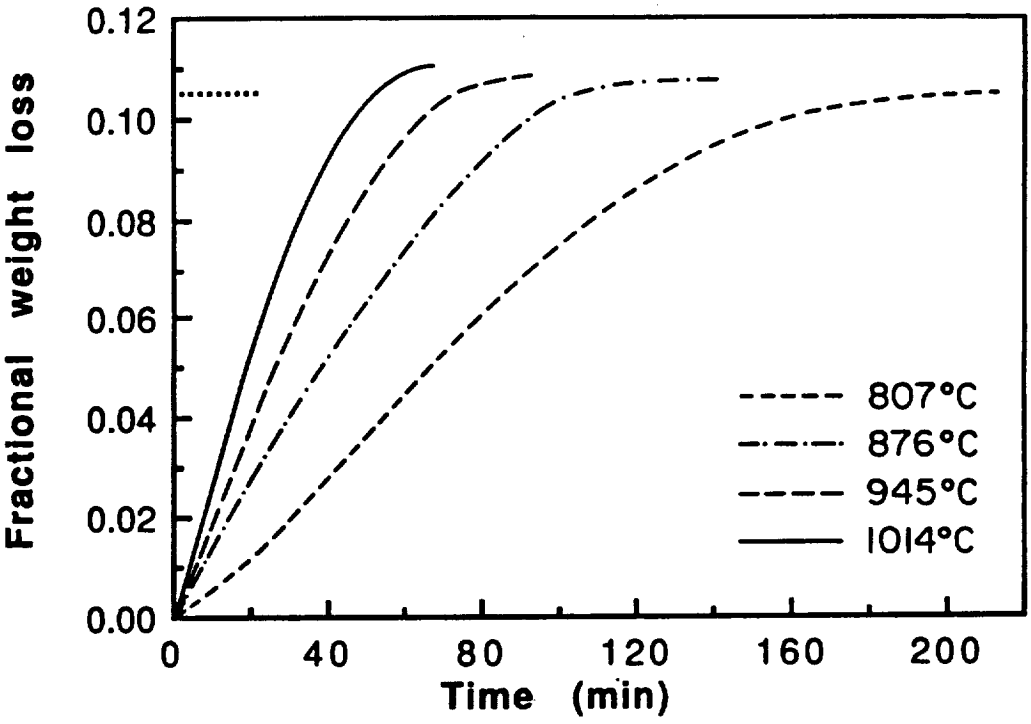

Figure 5. Effect of temperature on the reduction rate of ilmenite: H_2=3.4%; ·····, complete iron metallization

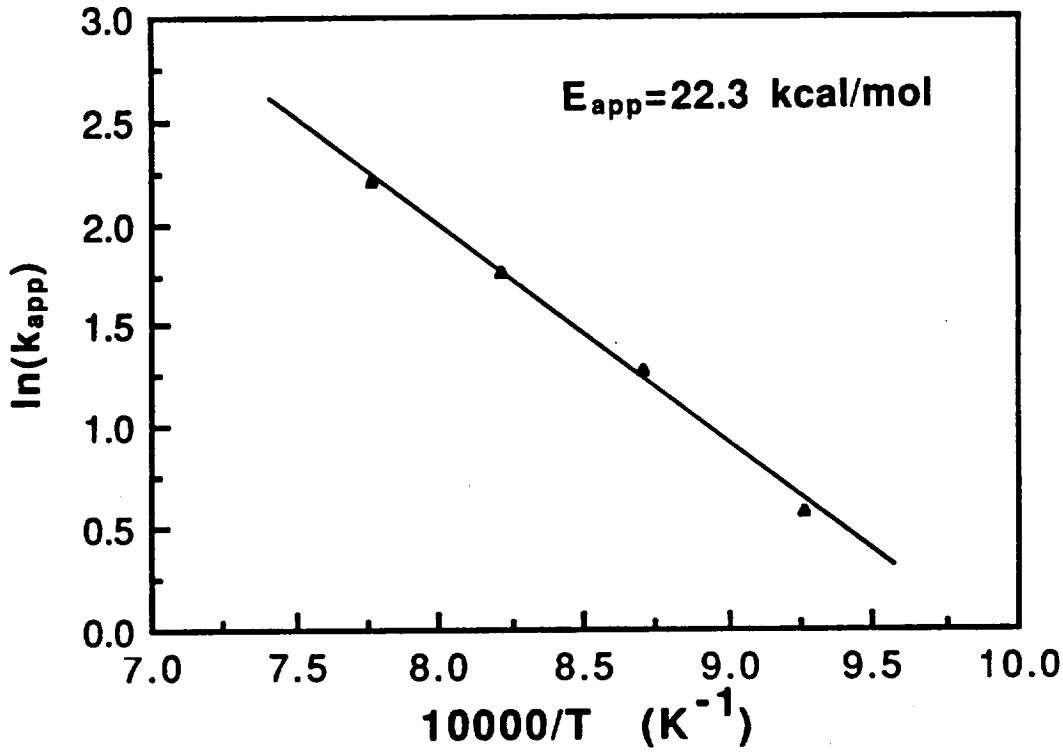

Figure 6. Temperature dependence of the apparent rate coefficient.

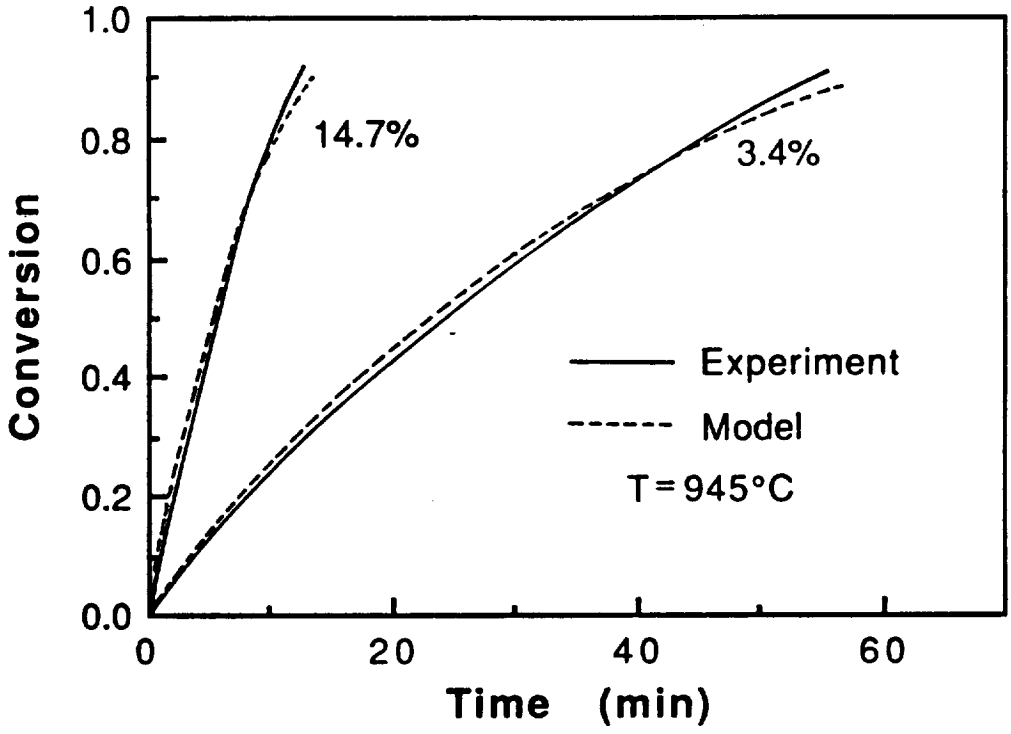

Figure 7. Comparison of experimental data with model predictions: H_2=3.4% and 14.7%.

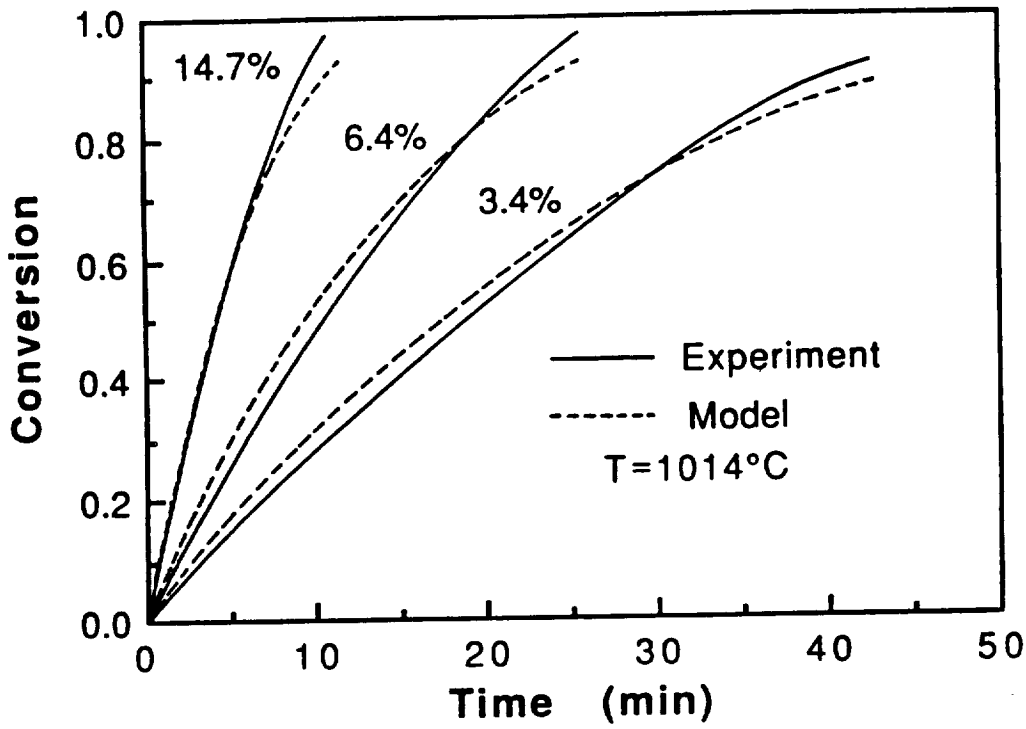

Figure 8. Comparison of experimental data with model predictions: H_2=3.4%, 6.4% and 14.7%.

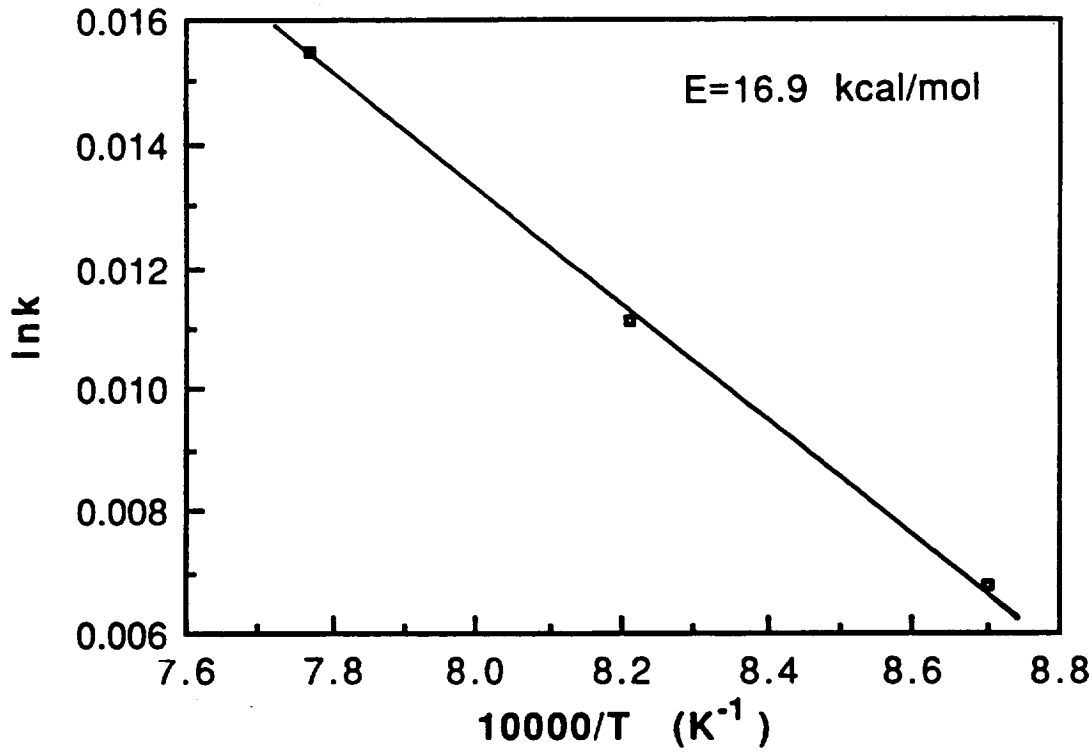

Figure 9. Temperature dependence of the intrinsic rate coefficient.

Figure 10a. Backscattered electron micrograph of the polished cross section of ilmenite flake after partial reduction, T=1014°C, Magnification=2000X.
Point concentrations in atom% are:

Point	Ti	Fe
1	50	50
2	51	49
3	51	49
4	2	98
5	96	4

Figure 10b. Fe kα X-ray map of the cross section shown in 10a.
Figure 10c. Ti kα X-ray map of the cross section shown in 10a.

Figure 11a. Backscattered electron micrograph of the polished cross section of ilmenite flake after partial reduction, T=807°C, Magnification=5000X.
Point concentrations in atom% are:

Point	Ti	Fe
1	50	50
2	50	50
3	51	49
4	5	95
5	99	1

Figure 11b. Fe kα X-ray map of the cross section shown in 11a.
Figure 11c. Ti kα X-ray map of the cross section shown in 11a.

Figure 12a. Backscattered electron micrograph of the polished cross section of ilmenite flake after complete iron metallization, T=945°C, Magnification=5000X.
Point concentrations in atom% are:

Point	Ti	Fe
1	99	1
2	99	1
3	2	98
4	3	97

Figure 12b. Fe kα X-ray map of the cross section shown in 12a.
Figure 12c. Ti kα X-ray map of the cross section shown in 12a.

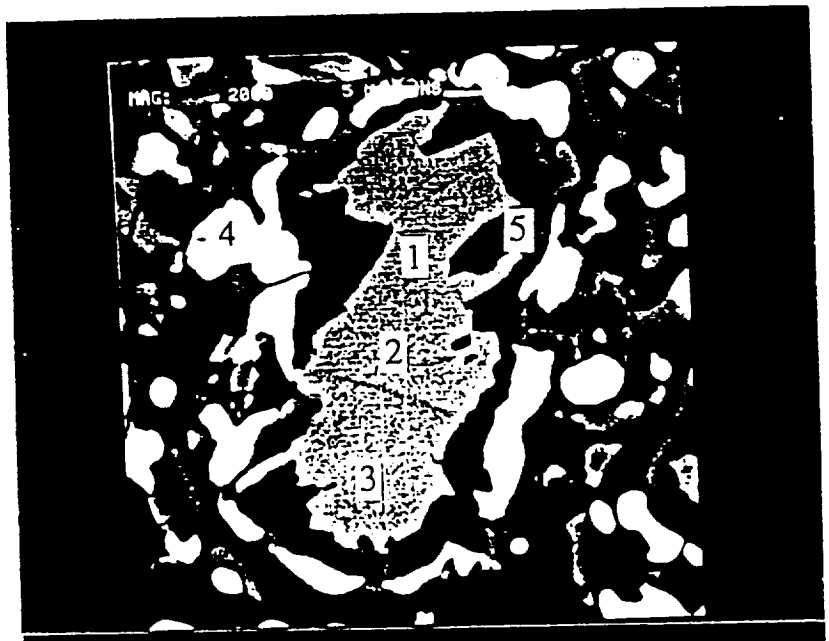

Figure 10a.

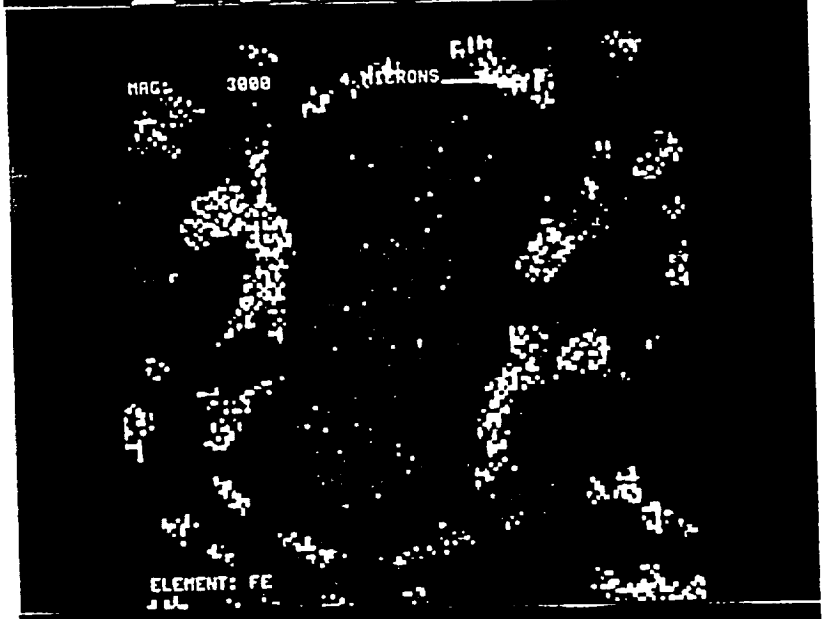

10b.

10c.

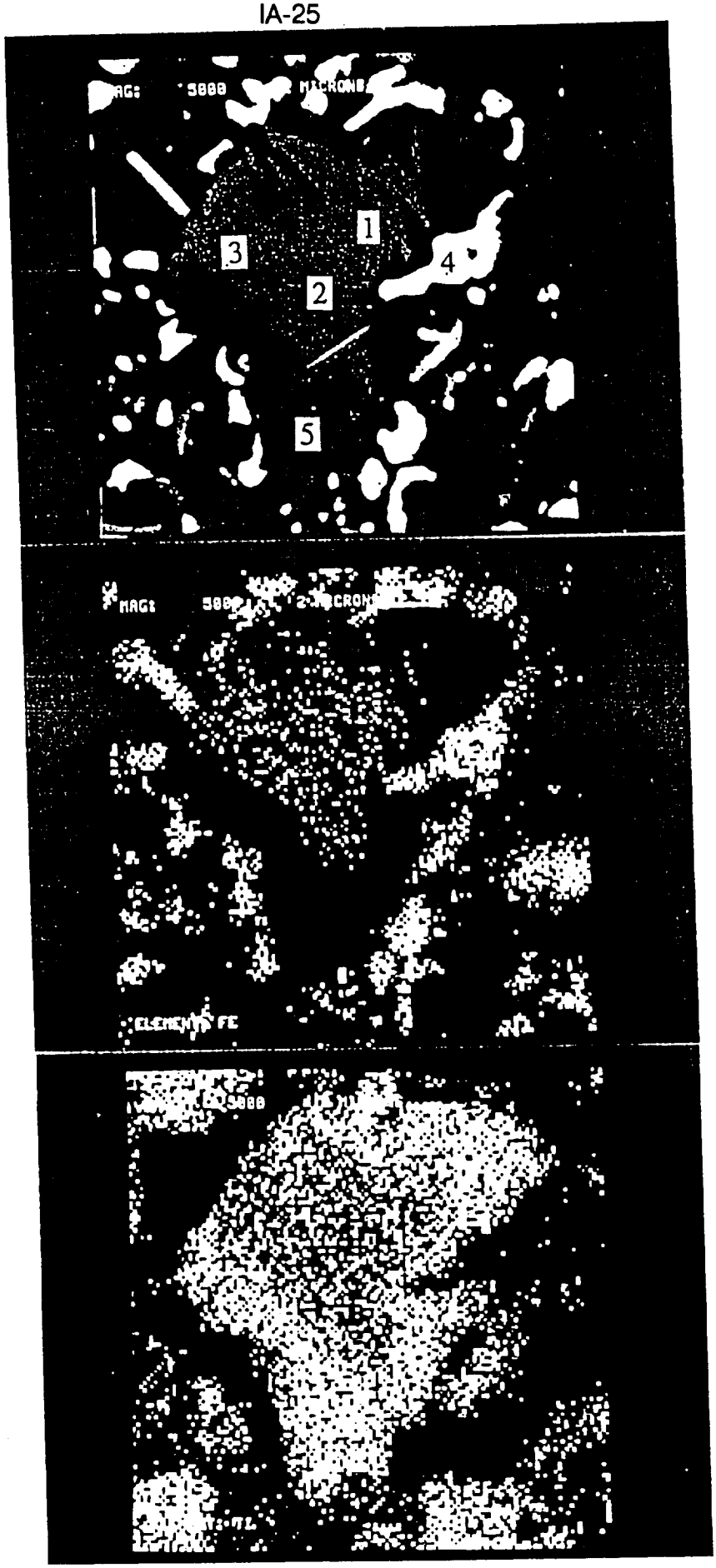

Figure 11a.

11b.

11c.

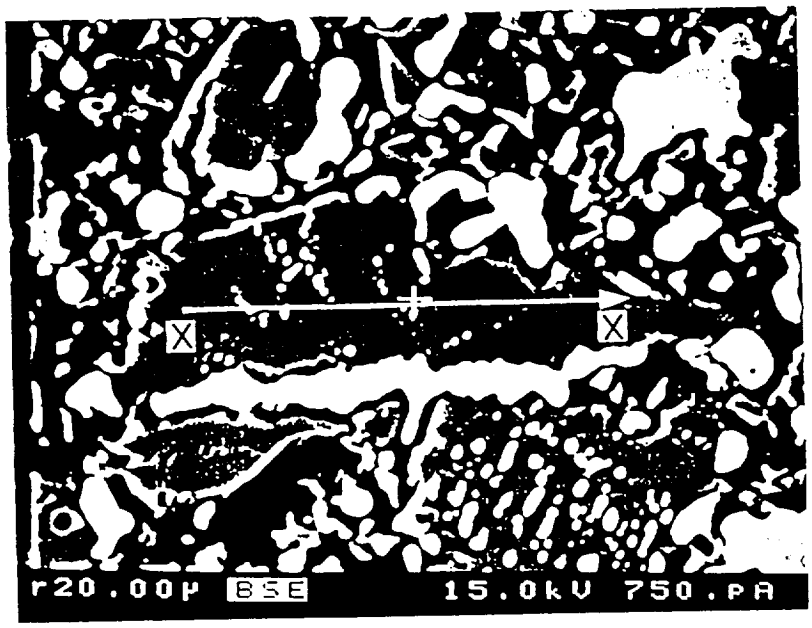

Figure 13. Backscattered electron micrograph of a reduced TiO_2 phase.

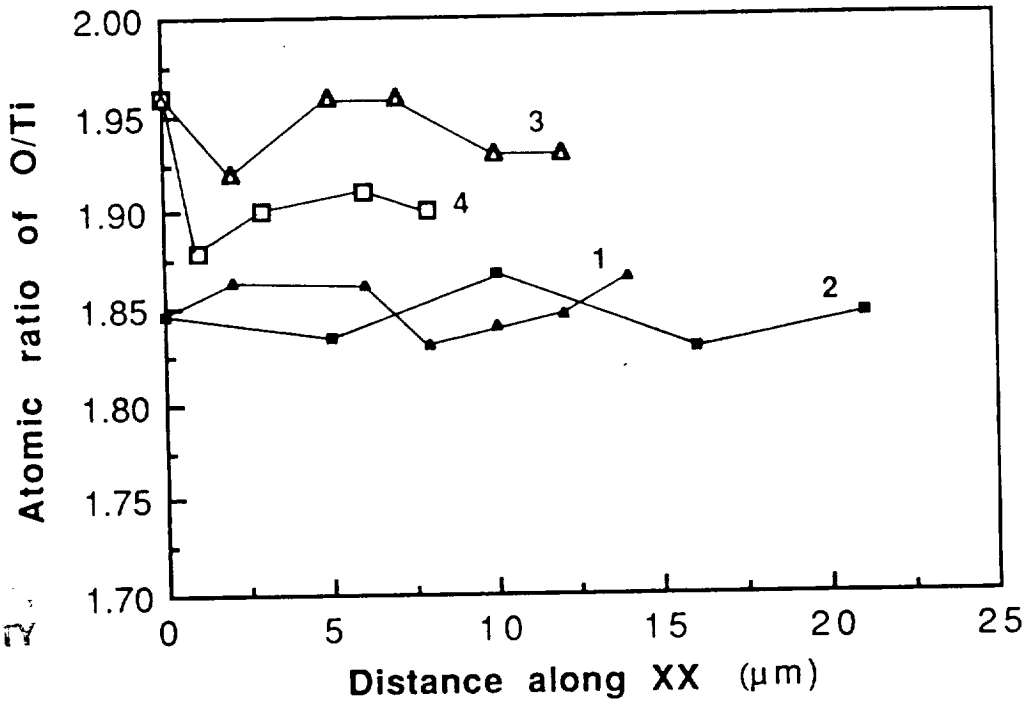

Figure 14. Variation in the oxygen to titanium atomic ratio in flakes.
1: sample 1, edge (Figure 13), T=1014°C
2: sample 1, center, T=1014°C
3: sample 2, edge, T=876°C
4: sample 2, center, T=876°C

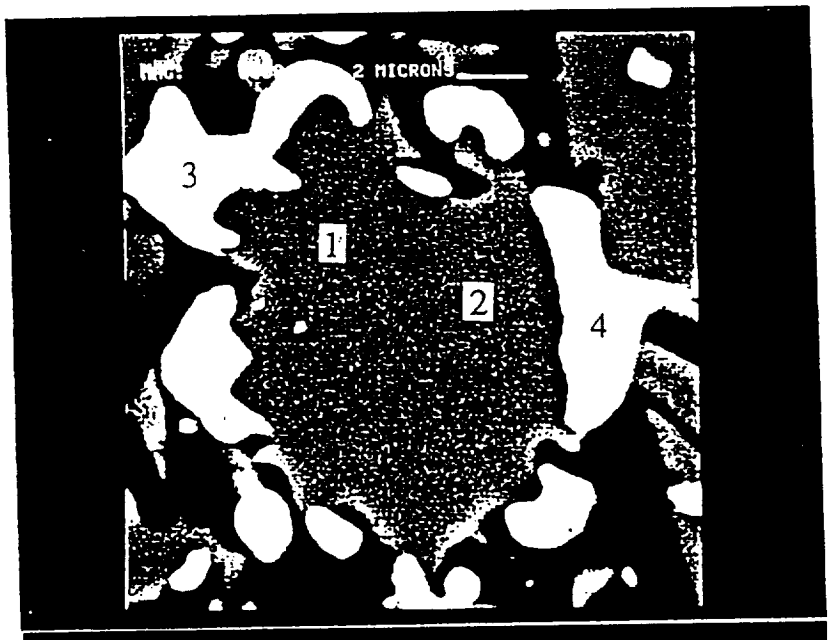

Figure 12a.

12b.

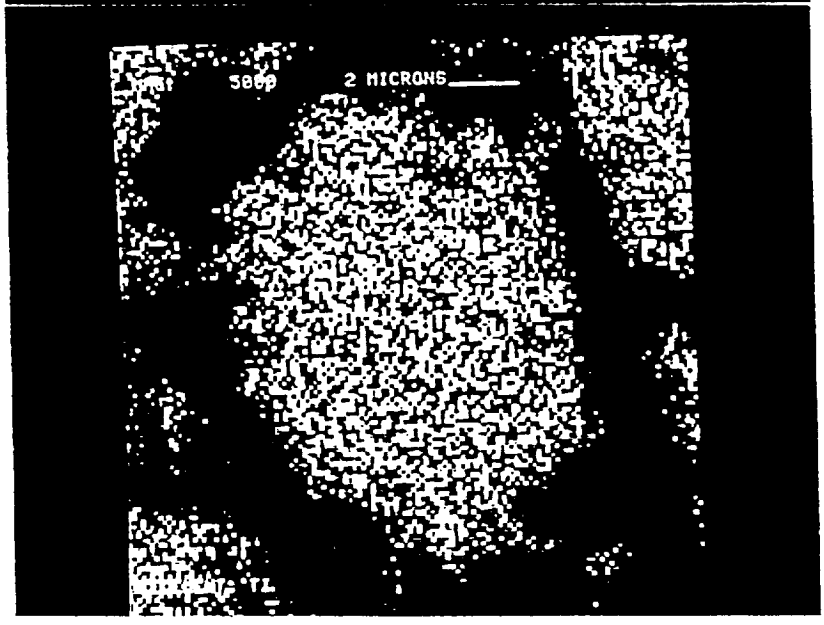

12c.

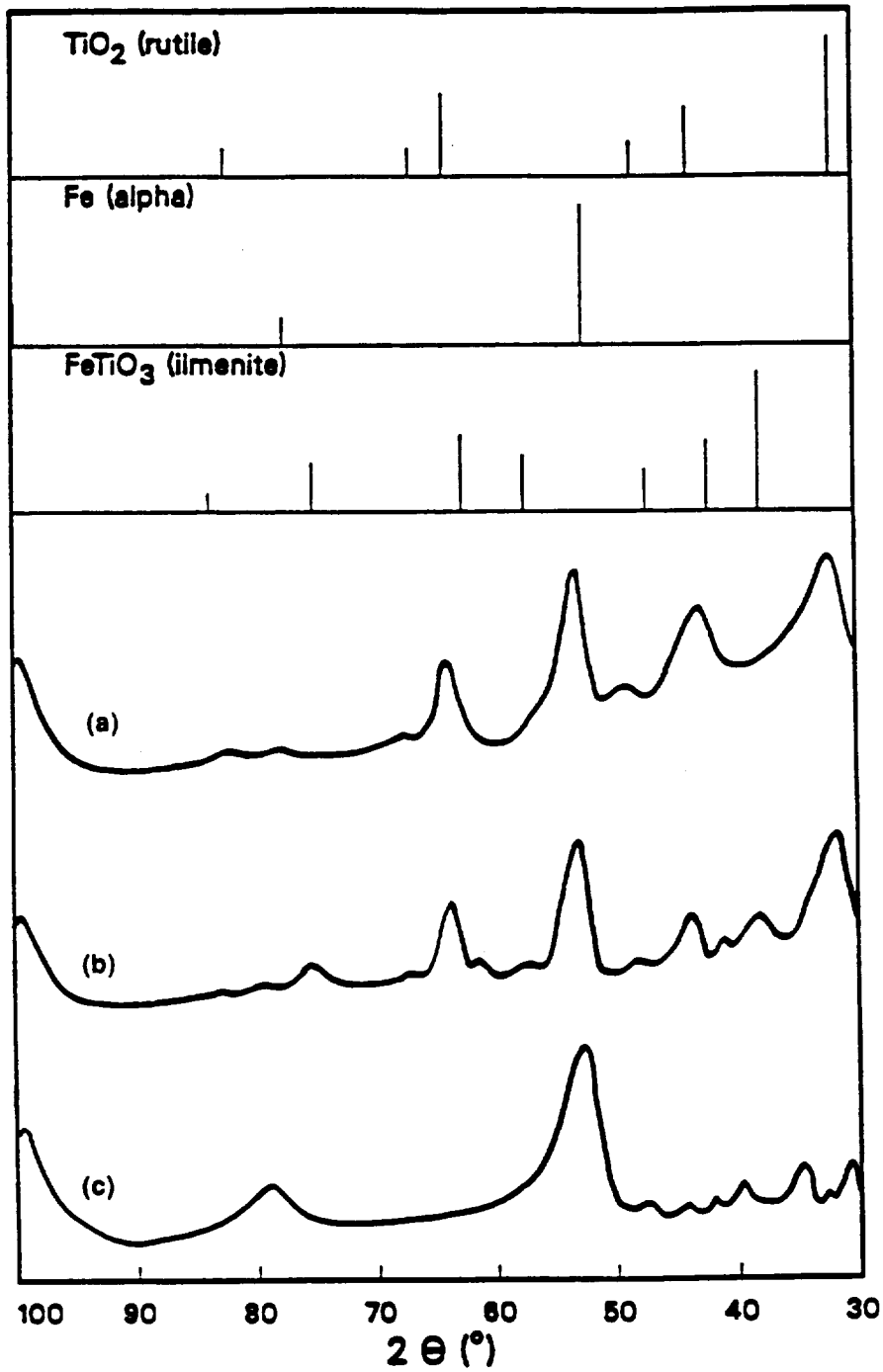

Figure 15. X-ray diffraction spectrum of:
a) ilmenite, complete iron metallization at 807°C.
b) ilmenite, partially reduced at 807°C or 1014°C.
c) ilmenite, complete iron metallization and partial reduction of TiO_2 at 876°C, 945°C and 1014°C.

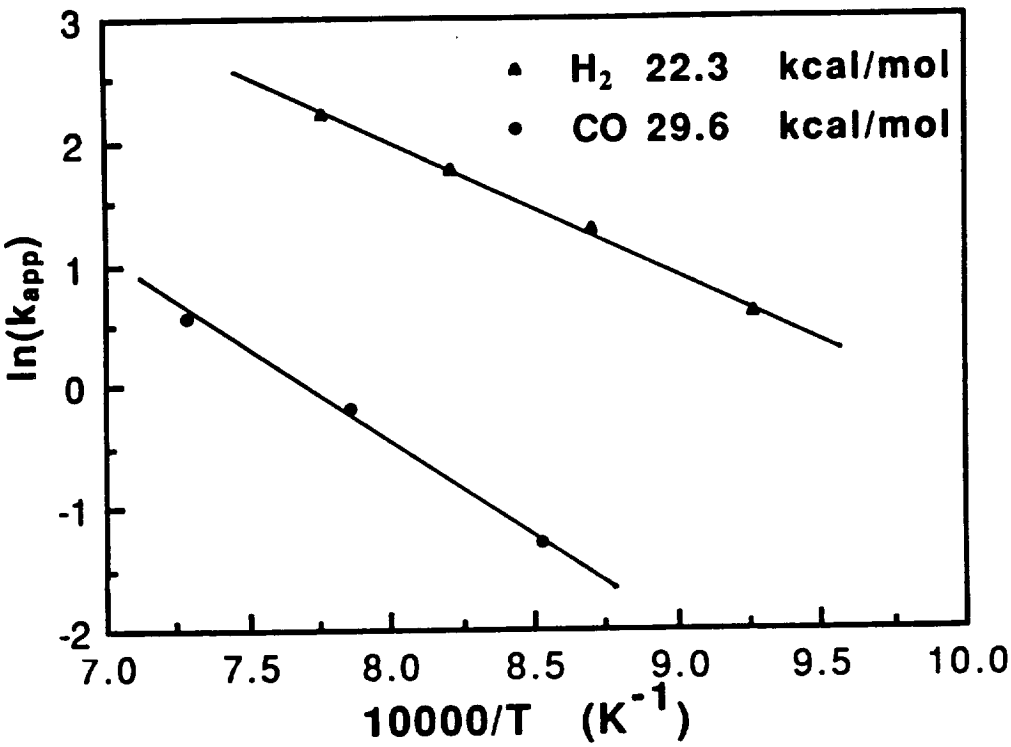

Figure 16. Temperature dependence of the apparent rate coefficient.

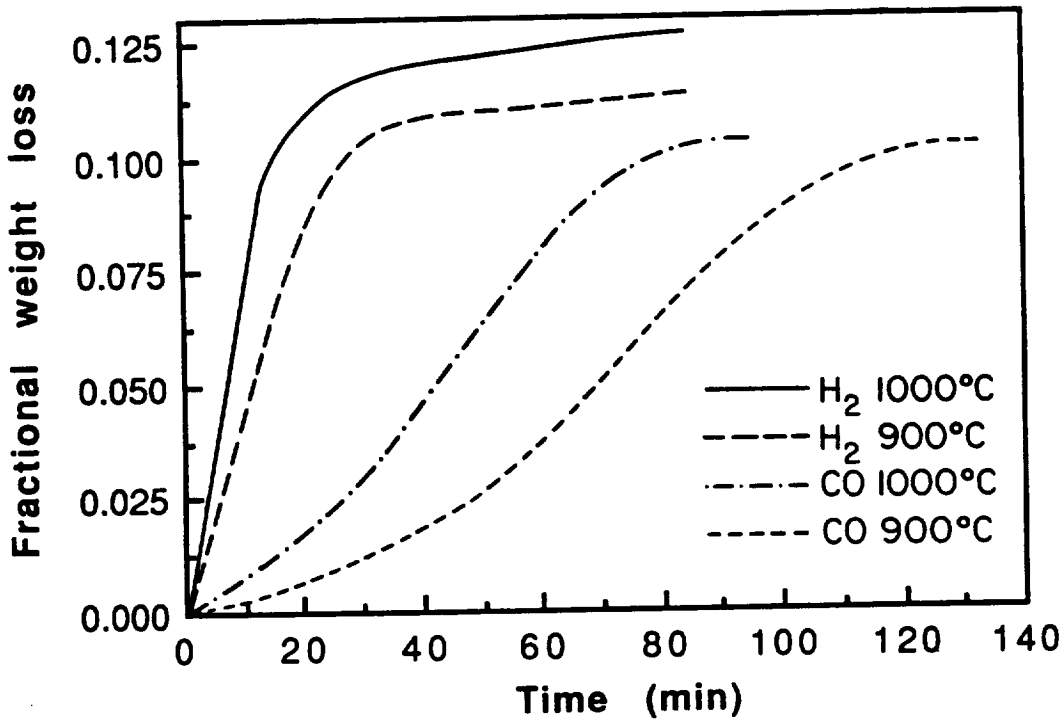

Figure 17. Effect of reducing agents on the reduction of ilmenite.

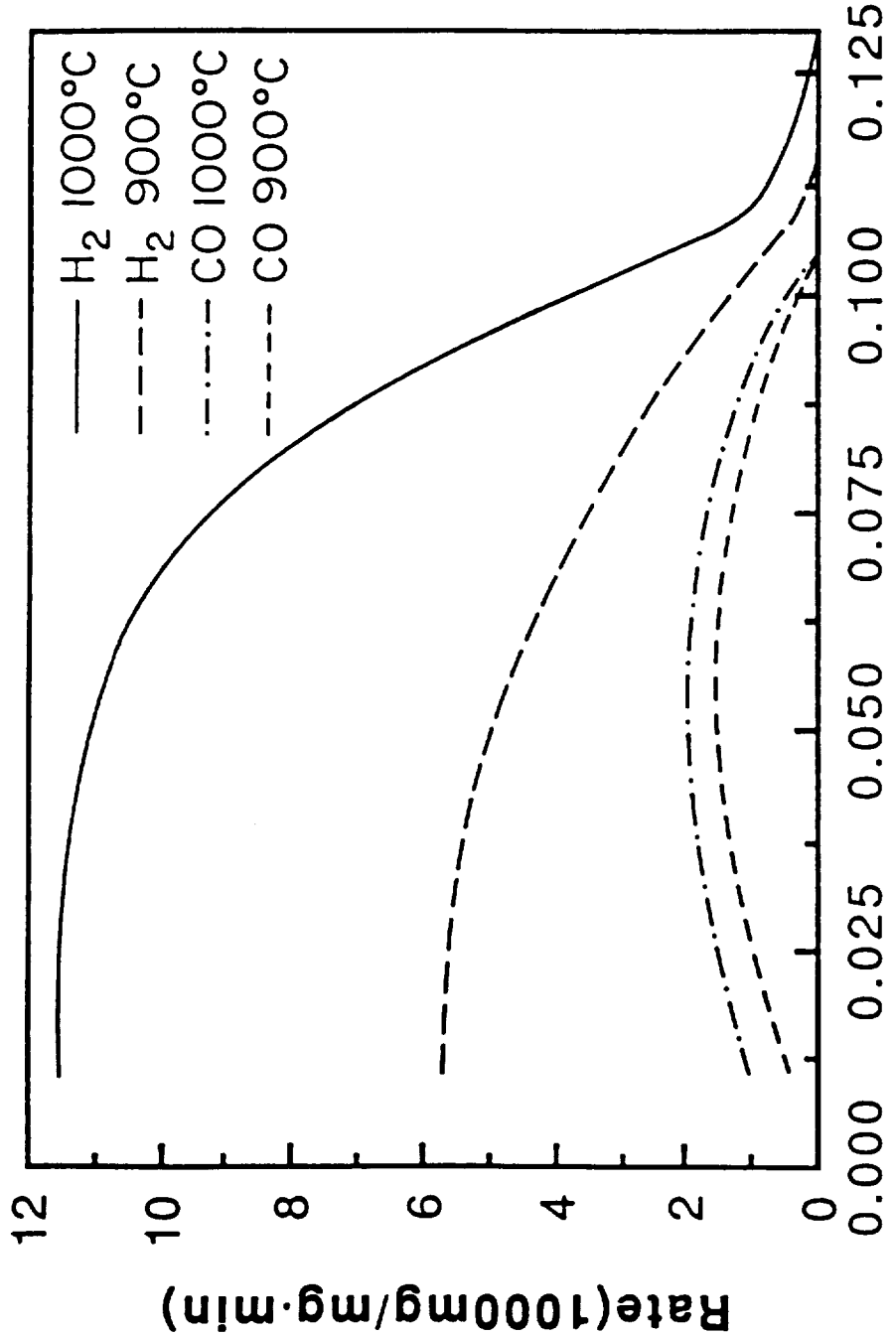

Figure 18. Effect of reducing agents on the reduction rate of ilmenite.

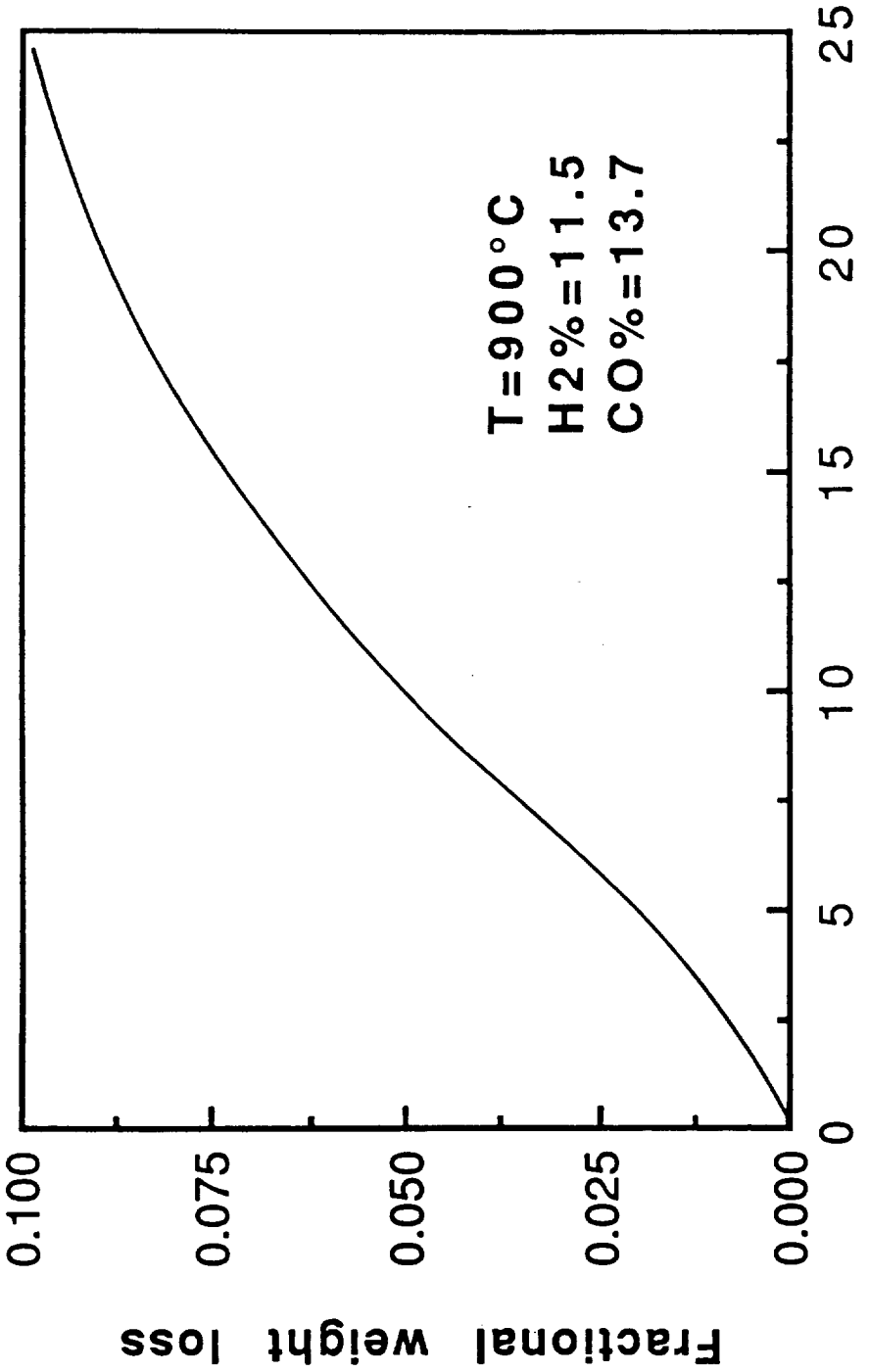

Figure 20. Reduction of ilmenite with H_2/CO mixture.

Non-slagging Carbothermal Reduction of Ilmenite

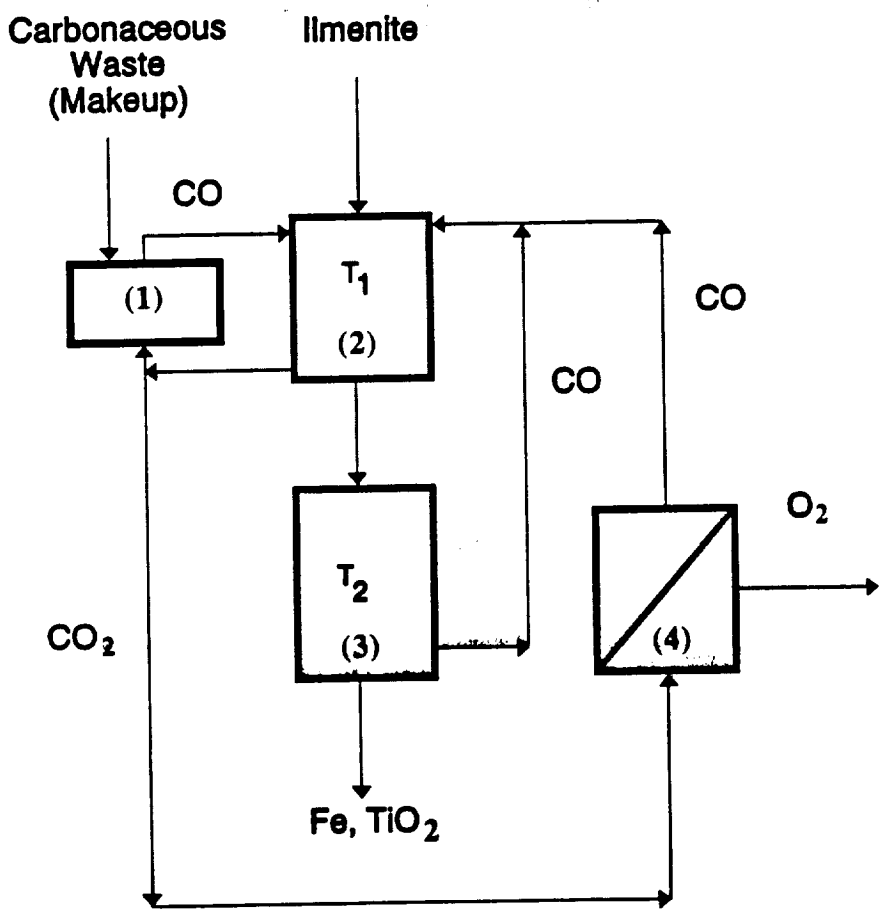

Figure 19. Flowsheet for a novel carbothermal reduction process.